5.1 IRRADIATION RESPONSE OF NEXT GENERATION HIGH TEMPERATURE SUPERCONDUCTING RARE-EARTH AND NANOPARTICLE-DOPED $YBa_2Cu_3O_{7-X}$ COATED CONDUCTORS FOR FUSION ENERGY APPLICATIONS - K.J. Leonard, T. Aytug, Fred. A List III, Yanwen Zhang (Oak Ridge National Laboratory),A. Perez-Bergquist, W.J. Weber (University of Tennessee), A. Gapud, N.T. Greenwood, J.A. Alexander and A. Khan (University of South Alabama)

OBJECTIVE

The goal of this work is to evaluate the irradiation response of the newest generation of coated conductors based on rare earth and nanoparticle doping of the $YBa_2Cu_3O_{7-x}$ (YBCO) high temperature superconductors. The materials under investigation represent different methods for enhanced flux pinning for improved performance under externally applied magnetic fields. Ion irradiation was used to perform an initial evaluation of the materials electrical response, and is currently being followed up by neutron irradiation testing.

SUMMARY

During this reporting period, electrical characterization work was completed on the ion irradiated superconducting films. Detailed electrical characterization of the materials response was performed at the University of South Alabama. This contribution highlights results of a forthcoming paper concluding the electrical characterization of the ion irradiated materials. Based on this work, the Zr-doped $(Y,Gd)Ba_2Cu_3O_{7-x}$ and $(Dy,Y)Ba_2Cu_3O_{7-x}$ (DyBCO) materials were selected for neutron irradiation studies. Ion irradiation results for the $GdBa_2Cu_3O_{7-x}$ conductor did not show a significant improvement over second-generation YBCO materials in terms of J_c improvement with irradiation. However, irradiated T_c remained higher than for YBCO. The neutron irradiation exposures are being planned for the July-August 2014 cycle at HFIR. Information on the irradiation capsules and preliminary results will be included in the next semi-annual report.

EXPERIMENTAL

The high temperature superconducting (HTS) coated conductors consisted of metal organic chemical vapor deposition Zr-doped $(Y,Gd)Ba_2Cu_3O_{7-x}$ (Zr-YBCO) and $GdBa_2Cu_3O_{7-x}$ (GdBCO) films fabricated by SuperPower Inc., and metal organic deposition Dy-doped $YBa_2Cu_3O_{7-x}$ (DyBCO) films processed by American Superconductor Corporation. The HTS conductors were fabricated in long-lengths, but with individual test samples sectioned from the processed tapes.

Ion irradiation of the HTS materials was performed at the University of Tennessee Ion Beam Materials Laboratory using 5 MeV Ni and 25 MeV Au ions. The energies were selected to provide a range of damage effects in order to examine conductor response. This range was also selected to avoid implantation in the conductor and avoid columnar defect formation, which appear at electron energy loss values (S_e) around 20 keV/nm (S_e, of the Ni and Au ions was 1.8 and 6 keV/nm, respectively). Irradiations were performed at room temperature, normal to the tape surfaces to fluences of 10^{11} and 10^{12} cm^{-2} for 25 MeV Au ions, producing 0.003 and 0.03 displacements per atom (dpa), and with $5.5x10^{11}$ cm^{-2} for 5 MeV Ni ions producing 0.004 dpa in the Zr-YBCO and GdBCO films and 0.005 dpa in the DyBCO films.

Transport measurements were performed at the University of South Alabama on 1.7 cm long samples patterned with a 1-mm-long, narrow bridge with a width of either 1.00 mm or 0.20 mm. For each current contact to the probe, a strip of indium was applied to the Ag pads at pressed copper injection areas, which limited the contact resistance to between ~ 10^{-6} and 10^{-4} Ω. The probe was placed in a variable-temperature cryostat with the field of a 9-Tesla superconducting magnet applied normal to the tape plane (approximately parallel to the crystal *c*-axis). Temperature- and field- dependence of resistivity, $\rho(T, H_o)$ was measured for each constant field H_o over a slow rate of change of temperature T, never more than 0.2 K/min, such that there was negligible difference between the data for cooling and for warming. Critical

temperature for each field, $T_c(H_o)$, was determined using the resistivity criterion of 10^{-9} Ωcm, and the locus of all points $T_c(H_o)$ constituting the irreversibility line in the range of fields H_o = 0 to 9 Tesla. For measurements of J_c, the system is designed to provide pulsed DC currents of up to 10 A, each with a duration of up to 50 ms, which, together with low contact resistance, effectively eliminates any significant joule heating [[1]]. Critical current was defined using the standard voltage criterion of 1 μV/cm.

RESULTS

An example of the temperature dependent resistivity in self-field is shown in Figure 1a for the Zr-YBCO conductor. This example represents a common trend of the normal-state resistivity of the conductors with resistivity increasing and critical temperature T_c decreasing with higher dpa. The residual resistivity, ρ_i, obtained from a fit to the $\rho \sim T^2$ portion of the curves extrapolated to the intercept at zero temperature as postulated in Mathiessen's Rule, $\rho = \rho_i + \rho_n(T)$ for the different irradiation conditions is shown for the Zr-YBCO, where ρ_n is the temperature dependent normal-state resistivity. The values for the GdBCO conductor where not obtainable through this method, due to the negative curvature of the plotted data, so resistivity at T=100K, or the ρ_{100} value were compared for the three conductors in Figure 1b. This figure also provides a summary of the changes in T_c, ρ_i and ρ_{100} values for the three conductors with irradiation. For doses up to 0.005 dpa changes are very modest. For the higher fluence 25 MeV irradiations to 0.03 dpa, T_c reduction was within 1% of the unirradiated value, with DyBCO having the smallest reduction of -0.3% and GdBCO with the larger of about -1%. A comparative plot of ρ_{100} data for the three conductors and traditional YBCO films grown on single crystal $SrTiO_3$ (STO) and irradiated by 6 MeV He, 25 MeV O, and 120 MeV Kr are shown in Figure 2. The values for electronic energy loss, S_e, for He and O irradiations were slightly lower than those of the 5 MeV Ni and 25 MeV Au, but resulted in a greater degradation in materials properties in the YBCO films. Values for nuclear energy loss, S_n, were greater in the case of the 5 MeV Ni and 25 MeV Au (0.29 and 1.4 keV/nm, respectively, compared to 0.02 keV/nm or less for other studies). Despite these higher values, the relative lack in property changes may be attributed to the reduced number of defect sites in the YBCO films grown on the single crystal STO substrates that include, grain boundaries, domain boundaries, intergrowths and secondary phases that act as sinks for irradiation damage. Furthermore, it has been also experimentally observed that the YBCO films are more sensitive to electronic interactions over that of nuclear [[2]]. The S_e/S_n ratios for the irradiations of this study are below 9, while the ratios for 25 MeV O and 6 MeV He are calculated at 100 and 1350, respectively. This difference between the irradiation responses of the conductors of this study to that of YBCO films on STO substrates is further evidenced by the changes in T_c as a function of dose. For 1 MeV Ne and 2 MeV Ar irradiations (S_e = 1.6 and 2.3 keV/nm, respectively) of YBCO films on STO, values of $-\Delta T_c/T_{co}$ were as high as 54 and 80%, respectively for dpa values near 0.026 [[3]]. Whereas, in this study, T_c fall-off was within 7% of the unirradiated values for all three conductors irradiated to 0.03 dpa. This is likely an effect of the high S_e/S_n values creating defect sites that may be different than those observed at lower ratios.

A plot of the change in critical current density, represented as the ratio of irradiated to unirradiated values (J_c/J_c^o) as a function of applied magnetic field is shown in Figure 3. The GdBCO conductors response to irradiation by 5 MeV Ni and 25 MeV Au up to 0.004 dpa is very similar and shows a slight decrease in the *H//c* properties up to 8 Tesla in comparison to the unirradiated values. At higher dpa, the properties show a significant drop mainly from the disappearance of the Gd_2O_3 nanoparticles dispersed along the *ab* directions in the conductor. The Zr-YBCO conductor shows somewhat interesting results, in that J_c values are reduced in the 0.003 dpa 25 MeV Au irradiated material and increase to near unirradiated values at the higher dose levels. As observed in the angular field dependence of critical current [[5]], along with transmission electron microscopy studies [[6]], there is a significant improvement in *H//ab* pinning due to the development of intergrowths at the interface of the $BaZrO_3$. However, there is also a loss in the length of the c-axis oriented $BaZrO_3$ particles which may lead to the reduction in low field properties at low damage levels that can be recovered on the formation of smaller radiation-induced defects that were observed at the higher dpa levels. The DyBCO conductor shows relatively unchanged values over the unirradiated condition up to 0.005 dpa at the low field conditions. However at high field, all irradiation

conditions show a large improvement over the unirradiated J_c values. Currently, efforts are underway to identify the defects or features responsible for the increase in the high field conditions.

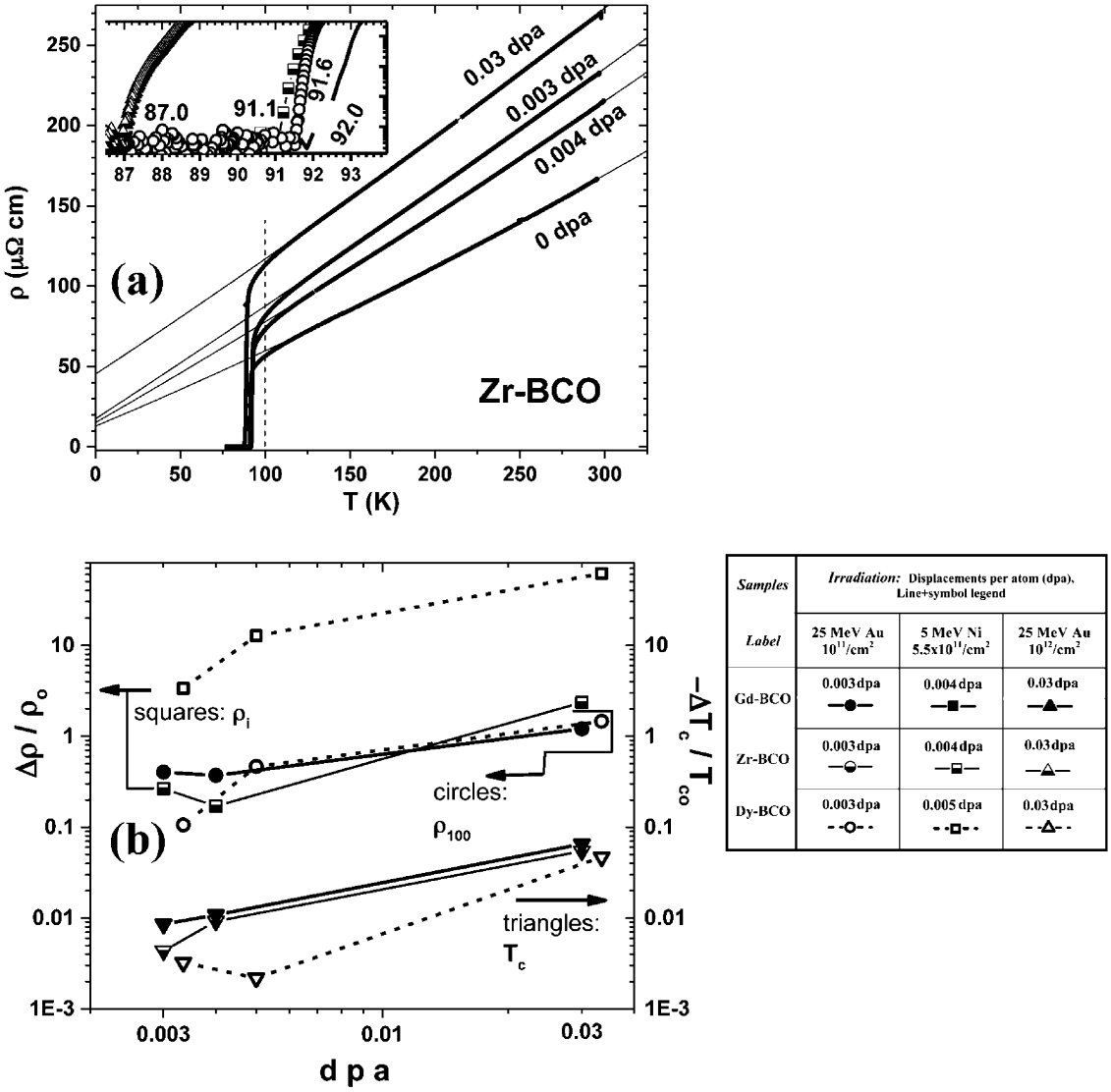

Figure 1. (a) Resistivity as a function of temperature and dpa for the Zr-YBCO conductor, with the intercept showing the residual resistivity (ρ_i) and resistivity at a temperature of 100 K (ρ_{100}). (b) Fractional shifts relative to the unirradiated state of the ρ_{100} value and the critical temperature T_c.

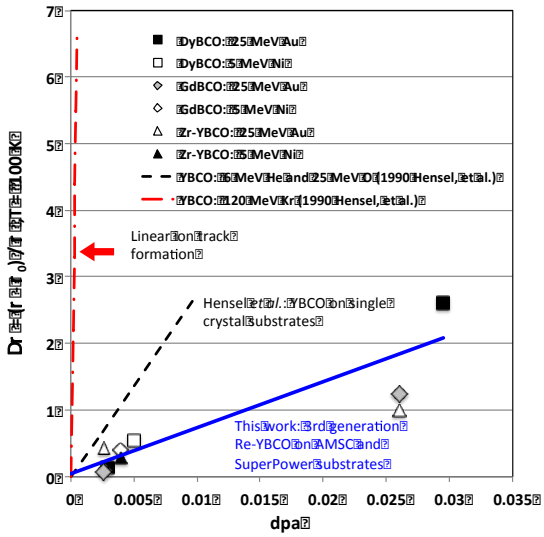

Figure 2. The ρ_{100} values as a function of dpa for the conductors of this study compared to that of YBCO films on single crystal $SrTiO_3$ [[2]]. Electron energy loss energies for the He and O ions are lower than that used in this study, while the 120 MeV Kr irradiation was at the known threshold that produces linear track formation in the YBCO film.

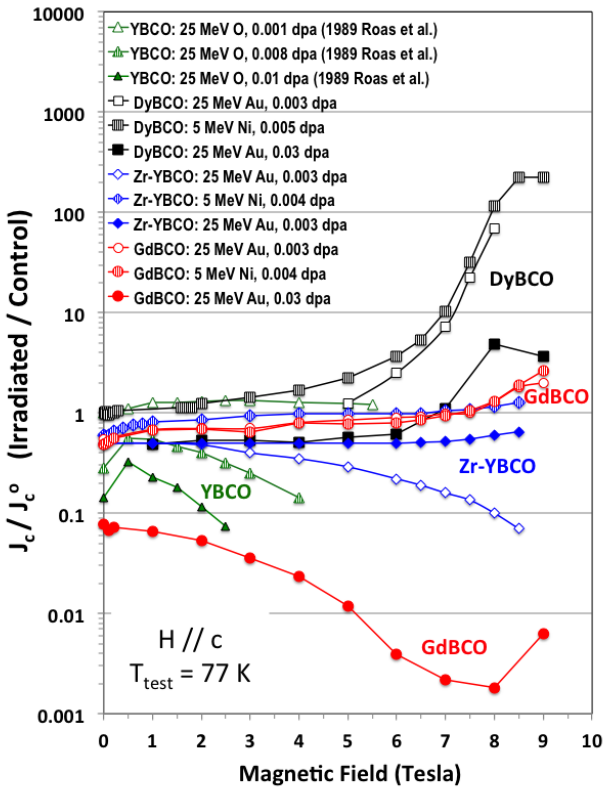

Figure 3. Plot of the changes in critical current density between the irradiated and unirradiated condition for the tested conductors as a function of applied magnetic field. Comparative data from YBCO films on STO substrates is also plotted [[4]].

As the changes in $J_c(H)$ correlate with the overall pinning force density ($F_p = J_cH$), there is normally a maximum pinning force F_p^{max} at a specific field condition. These are plotted as a function of dpa in Figure 4. Initial values of F_p^{max} are significantly higher for the DyBCO and Zr-YBCO conductors than that of the GdBCO, for all irradiation conditions except the low dpa 25 MeV Au irradiations. The field H_{max}, plotted also in Figure 1, is often associated with the "matching field" where the pinning structure becomes optimized for a certain applied flux. While H_{max} reduces for GdBCO with dose, there is an increase in the Zr-YBCO. However, the DyBCO is unique in that it shows a strong initial increase followed by decreasing values with dose, suggesting the pinning that is optimal for a specific field is not necessarily the strongest. There are clearly issues related to the pinning force and matching field that require further examination through microstructural examination.

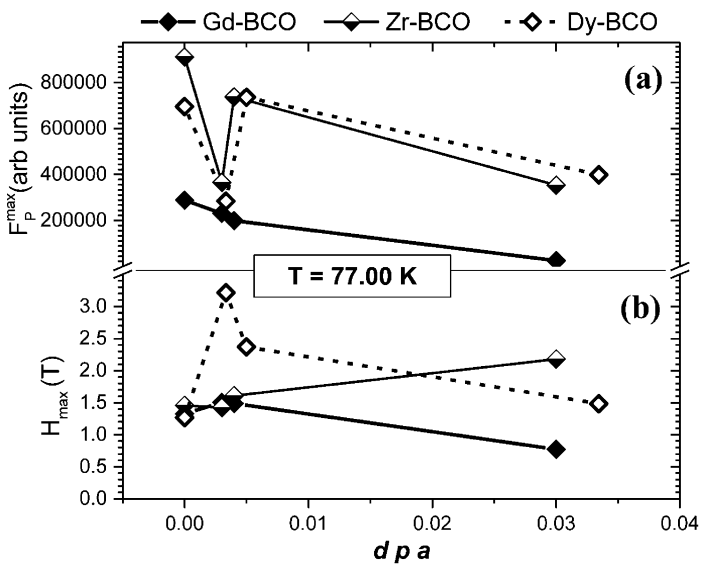

Figure 4. The dependence of the (a) maximum pinning force, F_p^{max}, and (b) the corresponding applied field H_{max} for the three conductors investigated.

The magnetic phase diagram, *H(T)* shown in the inset in Figure 5 for the DyBCO conductor, provides information on the irreversibility line (IL) between the state where vortices are free to move under the slightest applied current (vortex state) and the state where vortices are pinned ($J_c>0$). Also shown in the inset is the upper critical field $H_{c2}(T)$ as well as the IL line for a typical YBCO conductor (in red). The IL can be described as the depinning line, in which conditions to the left side of the line (lower H and T) vortices are pinned and the J_c is non-zero. The unirradiated DyBCO conductor shows a shift in the IL with respect to that of YBCO, with further enhancements observed with irradiation. However, at the high dose 25 MeV Au irradiation, the IL curve dips towards lower T_c values for given fields showing a loss in pinning at the low field conditions. The pinning is recovered above 6 Tesla as nanoscale radiation-induced defects observed through transmission electron microscopy become more favorable pinning locations at high fields.

The phase curves illustrating the change in the IL as a function of the percent shifted T_c are plotted for the three conductors studied in Figure 5. The line at $\Delta T=0$ demarcates between irradiation degradation ($\Delta T<0$) and enhancement ($\Delta T>0$). In general, a good correlation between the IL data and that of the $J_c(H)$ plots are observed. It can be further iterated that the low dose response of the GdBCO shows a slight reduction in the IL, but is further recovered at higher field strengths. However, significant degradation in the IL and $J_c(H)$ properties occurs following 0.03 dpa for the GdBCO. As observed in the $J_c(H)$ data, the IL data for the Zr-YBCO conductor shows a degradation occurring following just 0.003 dpa, believed to be related to the changes observed in the size distribution of the $BaZrO_3$ particles which are more effective in pinning at low applied fields. While there is not a significant difference in dpa between the 5 MeV Ni irradiations to 5.5×10^{11} cm^{-2} as compared to the 25 MeV Au irradiations to 1×10^{11} cm^{-2}, the Ni ions produce a larger S_e/S_n ratio than that of Au ions (8.6 compared to 4.8). This may create more ballistic mixing effects related to changes in the $BaZrO_3$ particles for the Au irradiations and less site occupancy defects within the matrix than is produced in the Ni irradiations. Furthermore, with ion irradiation performed normal to the tape surface, the c-axis aligned $BaZrO_3$ particles may be more sensitive than to irradiations performed at off angles, or by neutron irradiation. This is currently being examined through microstructural examination. As also demonstrated in the $J_c(H)$ data, the DyBCO data for the low fluence Au and Ni irradiations show an enhancement in pinning properties. Only the 0.03 dpa 25 MeV Au irradiation shows degradation in the low field properties that are quickly recovered above 6 Tesla. This suggests a substantial effect of ion irradiation on the Dy_2O_3 at high fluences, but with a substantial

improvement in *H//c*. It remains to be determined through microstructural analysis if any realignment of the Dy_2O_3 particles occurs with ion irradiation or if this enhancement also in part to intergrowth and defect formations in the matrix portion of the conductor.

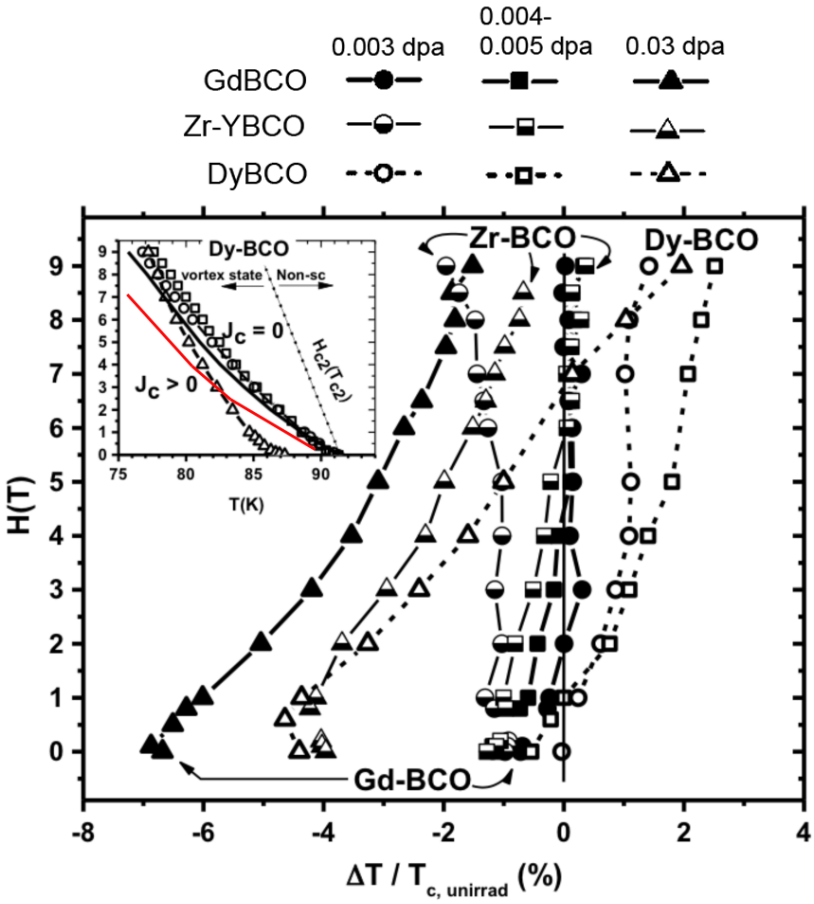

Figure 5. The changing irreversibility line versus the percent change in T_c as a function of irradiation exposure for the three conductors studied. The inset shows the irreversibility, upper critical field $H_{c2}(T)$ as well as the IL line for a typical YBCO conductor (in red) as compared to the data for the DyBCO conductor.

The vortex creep rate, *S*, can be calculated for T=77 K through the power law relationship between the voltage associated with dissipative vortex motion and the applied current ($V \propto I^n$). Where *n* is the slope of the same *logV-logI* curves used in determining the Ic at T=77 K, with the analysis being only performed to the lowest irreversibility field for dpa < 0.03 at this temperature which is 7.5 Tesla. The relationship [[7],[8]] between the power law relationship and the vortex creep rate is found in the conjunction with the Maxwell Equation, $V \propto -\frac{d\phi}{dt} \propto -\frac{dI}{dt}$, which leads to the vortex creep rate, $S = -\frac{dlnI}{dlnt} = \frac{1}{n-1}$. The normalized vortex creep rate for the irradiated conductors at T =77 K is shown in Figure 6. A lower vortex creep rate is favorable as it demonstrates the stability of the pinning centers in the material. Therefore, for the normalized creep rate, the greater the value above unity the less favorable. As expected the high dose GdBCO has the highest *S* value at low applied fields due to the loss of the Gd_2O_3 particles in the conductor film. At lower damage levels the GdBCO and Zr-YBCO conductors behave comparable to the unirradiated material. However, the value of *S* is lower in the irradiated DyBCO films following irradiation.

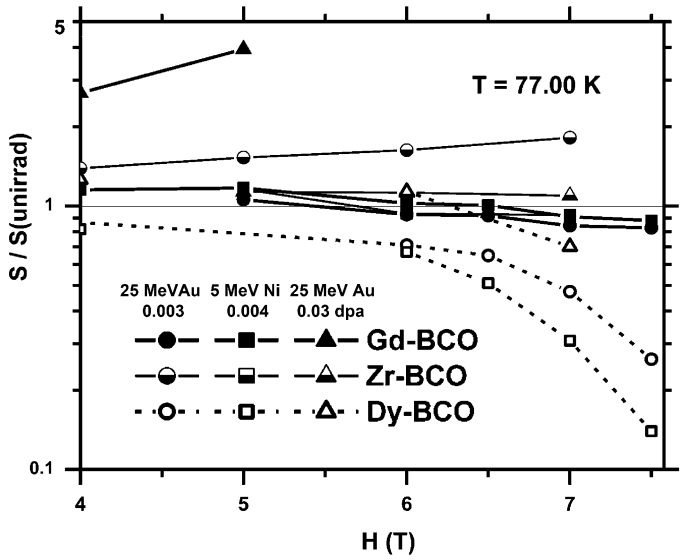

Figure 6. The normalized vortex creep rate as a function of applied field for the various irradiation conditions.

CURRENT AND FUTURE WORK

Current work being performed involves investigating the microstructural link between the changes observed between the unirradiated and irradiated materials. The work on the GdBCO conductor is completed, while specific issues regarding the DyBCO and Zr-YBCO conductors are being addressed through further high-resolution electron microscopy at the Advanced Characterization Laboratory at ORNL. Specific issues currently being investigated through aberration corrected and more conventional TEM methods include the nature of the small radiation-induced stacking-fault-like defects observed in the high fluence 25 MeV Au irradiation, the initial drop in pinning force with irradiation observed in both the Zr-YBCO and DyBCO conductors. Related to the later is the investigated of the differences between the lower fluence 5 MeV Ni and 25 MeV Au irradiations and how the difference in S_e/S_n ratio affects the microstructures in each very different conductor.

Current work that will continue involves the first neutron irradiation testing of these materials. Specially designed capsule inserts have been built to accommodate the tape samples and to allow for controlled handling and processing of the samples through the irradiation and post-irradiation testing. Samples are expected to undergo irradiation in the July-August 2014 HFIR schedule. Irradiation capsules will be initially cut open at the hot cell, but with the internal holders sent to LAMDA for further disassembly and post-irradiation examination. Basic electrical characterization is planned along with TEM examination of the microstructures.

REFERENCES

[1] V. Rouco, E. Bartoloma, A. Palau, M. Coll, X. Obradors and T. Puig, Superconductor Science and Technology, 25 (2012) 122001.
[2] B. Hensel, B. Roas, S. Henke, R. Hopfengartner, M. Lippert, J.P. Strobel, M. Vildic and G. Saemann-Ischenko, Phys. Rev B42, 7, 4135 (1990).
[3] G.J. Clark, A.D. Marwick, R.H. Koch and R.B. Laibowitz, Appl. Phys. Lett. 51 (1987) 139.
[4] B. Roas, B. Hensel, G. Saemann-Ischenko, and L. Schultz, Appl. Phys. Lett., 54, (1989) 1051.
[5] K.J. Leonard, T. Aytug, A.A. Gapud, F.A. List III, N.T. Greenwood, Y. Zhang, A.G. Perez-Bergquist and W.J. Weber, Fusion Science and Technology, (2014) awaiting publication.

[6] K.J. Leonard, ORNL Fusion Materials Program Semi-annual, summer 2013.
[7] J.R. Thompson, Ö Polat, D.K. Christen, D. Kumar, P.M. Martin and J.W. Sinclair, Applied Physics Letters 93 (2008) 042506.
[8] H. Yamasaki and Y. Mawatari, IEEE Transactions on Applied Superconductivity, 9 (1999) 2651.